

# QED Calculation of the Quark Mixing Matrix

Peter Cameron\*

*Michigan/MIT/Brookhaven (retired)*

(Dated: January 27, 2025)

## Abstract

Many years ago Pierre Ramond suggested using the electromagnetic impedance model to calculate neutrino PMNS and quark CKM mixing matrices [1–4]. Given the long-dreaded desert at the LHC (one Higgs and no SUSY), motivated in no small part by Carlo Rubbia’s call for courage [5], and with neutrino oscillation in the foreground for both experimentalists and theorists, neutrinos took precedence over quarks in following Pierre’s guidance. That focus led to conjecture on the role of neutrinos in low energy muon lifetime enhancement [6, 7], complementary to high energy relativistic time dilation of the Muon Collider proposal [8]. Serendipity recently offered a hand up, when it was realized that precise amplitudes emerging from the quantum impedance network neutrino mixing calculations appear to be not of neutrinos, but rather the closely related quark mixing. What follows presents details of the quark mixing matrix calculation, and outlines an earlier similar QED calculation of  $\pi^0$ ,  $\eta$ , and  $\eta'$  branching ratios.

*“To understand the electron would be enough”*

*Einstein*

Hans Dehmelt, 1989 Nobel Prize Lecture

## Outline

1. Introduction
  2. Quark mixing matrix impedance calculation
  3. Wolfenstein Parameters
  4. Unitarity, Cabibbo angle, and RMS variation
  5. CP violation, spin, dimensionality, and topology
  6. Topological calculation of  $\pi^0$ ,  $\eta$ , and  $\eta'$  branching ratios
  7. Summary
  8. Conclusion
- Acknowledgments
- Supplementary Material
- References

---

\* petethepop@aol.com

# 1. Introduction

The CKM matrix describes mixing between quarks in the Standard Model framework. It quantifies how quark ‘flavors’ change during electroweak interactions mediated by W bosons. The matrix is unitary, ensuring conservation of probability. It encodes CP violation (asymmetry between matter and antimatter) through a complex phase in its elements. The Standard Model CKM matrix result is derived using:

Experimental Data: Measurements of decay rates, mixing, oscillations, and CP violation.

Theoretical Inputs: Lattice QCD, effective field theories, and higher-order corrections.

Global Fits: Statistical analyses combining all inputs under the unitarity constraint.

This synergy of experiment and theory yields high precision:

$$\begin{bmatrix} |V_{ud}| & |V_{us}| & |V_{ub}| \\ |V_{cd}| & |V_{cs}| & |V_{cb}| \\ |V_{td}| & |V_{ts}| & |V_{tb}| \end{bmatrix} = \begin{bmatrix} .97435 \pm 0.00016 & 0.22500 \pm 0.00067 & 0.00369 \pm 0.00011 \\ 0.22486 \pm 0.00067 & 0.97349 \pm 0.00016 & 0.04182^{+0.00085}_{-0.00074} \\ 0.00857^{+0.00020}_{-0.00018} & 0.04110^{+0.00083}_{-0.00072} & 0.999118^{+0.000031}_{-0.000036} \end{bmatrix}$$

FIG. 1. CKM matrix amplitudes as presented by the 2024 Particle Data Group [4]

Matrix elements are amplitudes for transitions between up-type (u,c,t) and down-type (d,s,b) quarks. Amplitude squared (energy is square of field strength) gives the probability of up-type transforming into down (or down to up), with larger values for transitions within the same generation and smaller for inter-generational transitions. The CKM matrix is essential for understanding phenomena like decay rates, quark sector CP violation, and meson mixing.

The 2024 Review of Particle Physics CKM analysis [4] gives a profound sense of the monumental effort behind data presented in figure 1. In stark contrast, the impedance model result in blue italics of figure 2 was generated by nothing more than the electromagnetic coupling constant  $\alpha = e^2/4\pi\epsilon_0\hbar c$  and far-field photon scale-invariant topological impedance  $Z_0 = \sqrt{\mu_0/\epsilon_0}$ . If not serendipitous coincidence, then this seems most remarkable.

What follows presents figure 2 calculations and results for unitarity, Cabibbo angle, and Wolfenstein parameterization. Largest variances between data and model, the pivotal  $V_{us}$  Cabibbo angle and  $V_{cb}$  of Wolfenstein  $A$ , are discussed.

Similarities and differences of a previous topological calculation of  $\pi^0$ ,  $\eta$ , and  $\eta'$  branching ratios are outlined [9, 10].

	<b>d</b>	<b>s</b>	<b>b</b>
<b>u</b>	<b>0.9744</b> <i>ud <math>\pi^+</math></i> <b>0.9688</b>	<b>0.2251</b> <i>us <math>K^+</math></i> <b>0.2454</b>	<b>0.0037</b> <i>ub <math>B_u^+ ?</math></i> <b>0.0049</b>
<b>c</b>	<b>0.2249</b> <i>cd <math>D^+</math></i> <b>0.2454</b>	<b>0.9735</b> <i>cs <math>D_s^+</math></i> <b>0.9694</b>	<b>0.0418</b> <i>cb <math>B_c^+</math></i> <b>0.0347</b>
<b>t</b>	<b>0.0086</b> <i>td n/a</i> <b>0.0037</b>	<b>0.0411</b> <i>ts n/a</i> <b>0.0348</b>	<b>0.9991</b> <i>tb n/a</i> <b>0.9994</b>

FIG. 2. Data (black) and model (blue)

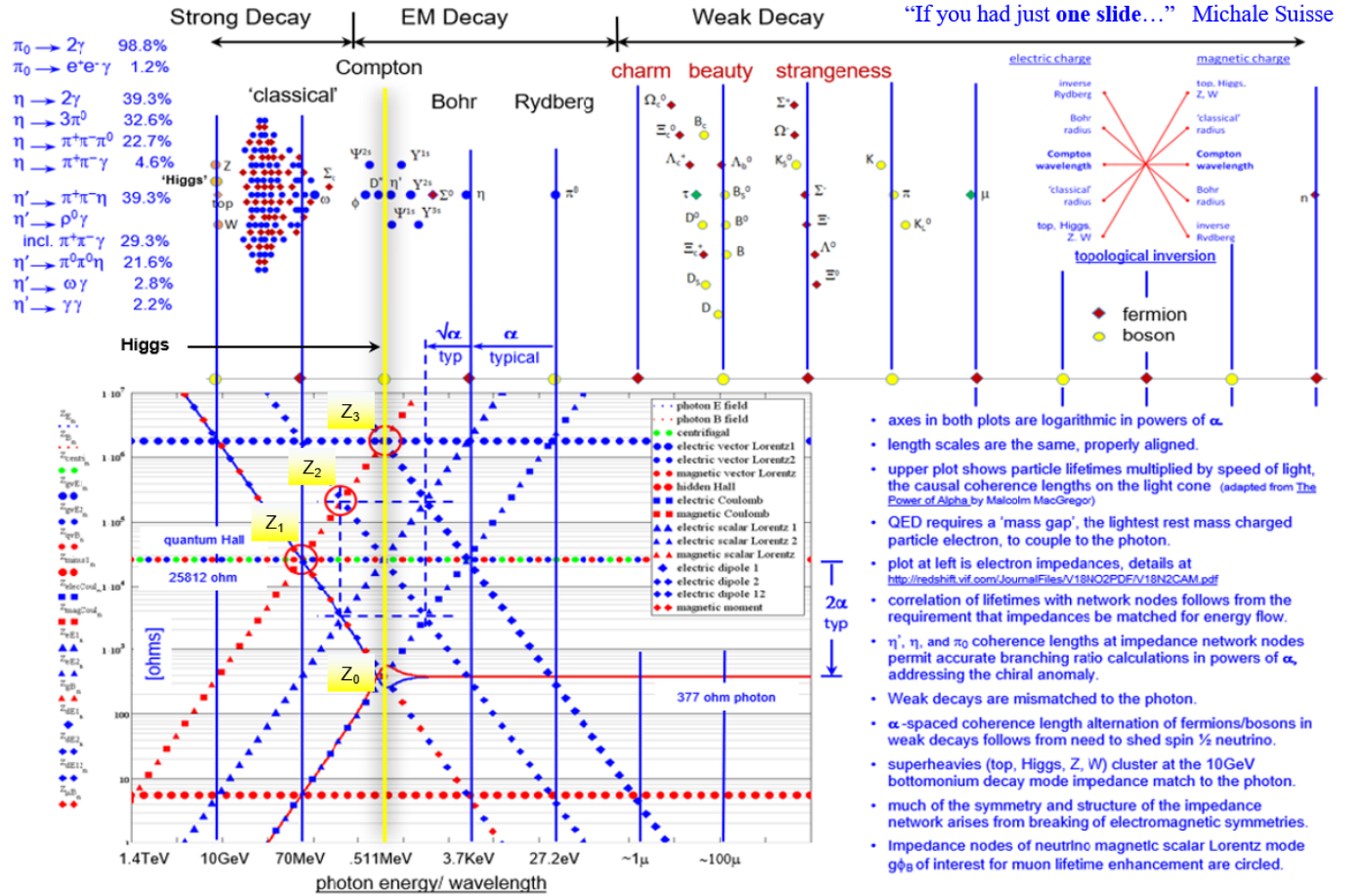
## 2. CKM matrix impedance calculation

$$\begin{aligned} Z_3 &:= \frac{Z_0}{(2\alpha)^2} & Z_3 &= 1.7686 \times 10^6 \text{ ohm} \\ Z_2 &:= \frac{Z_0}{(2\alpha)^{1.5}} & Z_2 &= 2.1367 \times 10^5 \text{ ohm} \\ & & & \text{quantum Hall, centrifugal,...} \\ Z_1 &:= \frac{Z_0}{2\alpha} & Z_1 &= 2.5813 \times 10^4 \text{ ohm} \\ & & & \text{photon far field} \\ Z_0 &:= \sqrt{\frac{\mu_0}{\epsilon_0}} & Z_0 &= 3.7673 \times 10^2 \text{ ohm} \end{aligned}$$

FIG. 3. CKM and PMNS impedances

The four quantum impedances used to calculate model amplitudes of figure 2 are shown in figure 3.  $Z_0$  is the 377 ohm far-field impedance the photon excites from the vacuum, square root of the *ratio* of magnetic permeability and electric permittivity. Square root of their *product* is speed of light. Photon is apparently the only particle that has both scale-invariant topological far-field and scale-dependent geometric near-field impedances. The remaining three impedances used to calculate the mixing matrix are generated as shown, by powers of twice the dimensionless coupling constant  $\alpha$ . They are relevant to both quark and neutrino mixing.

Locations of these four impedances in the .511 MeV QED mass gap impedance network [11–14] are shown in figure 4. In the model the three circled nodes are those of both the quarks' *magnetic* Coulomb mode (red squares) and neutrinos' *magnetic* scalar Lorentz mode (red triangles) [15]. This explains how seeking the neutrino mixing matrix serendipitously gives us quark mixing amplitudes. The Coulomb and scalar Lorentz impedances are capacitive. They couple with the inductive dipole modes at the three circled nodes.



Correlation of unstable particle lifetimes with network nodes follows from the fact that impedances must be matched for reflectionless energy flow during wavefunction decoherence

FIG. 4. The ‘One Slide’

The calculation takes phases of topological impedances  $Z_0$  and  $Z_3$  at the .511 MeV mass gap of QED to be absolute rather than relative, an absolute phase reference, a gauge fixing to the mass gap.

As shown in figure 5, both  $Z_0$  and  $Z_3$  appear in arguments of all six trig functions,  $Z_0$  in the numerator and  $Z_3$  in denominator. This calculates phase shifts between  $Z_0$  and  $Z_1$ ,  $Z_0$  and  $Z_2$ , and  $Z_0$  and  $Z_3$  relative to the mass gap at  $Z_3$ . These are non-linear. Shift from  $Z_0$  to  $Z_1$  is about 1 degree, 7 degrees to  $Z_2$ , and 89 degrees to  $Z_3$ .

In figure 5 results, sum of sine and cosine angles is  $\pi/2$ , as required by quadrature of Maxwell's equations in QED. Numerical values of sine and cosine are the same, of consequence in calculating not phase relative to the mass gap at  $Z_3$ , but rather phase shifts between the three nodes  $Z_1, Z_2,$  and  $Z_3$ .

$\phi_{\text{as}103} := \text{asin}\left(\frac{Z_1 - Z_0}{Z_3}\right)$	$\phi_{\text{as}203} := \text{asin}\left(\frac{Z_2 - Z_0}{Z_3}\right)$	$\phi_{\text{as}303} := \text{asin}\left(\frac{Z_3 - Z_0}{Z_3}\right)$
$\phi_{\text{as}103} = 8.2404 \times 10^{-1} \text{ deg}$	$\phi_{\text{as}203} = 6.9265 \times 10^0 \text{ deg}$	$\phi_{\text{as}303} = 8.8817 \times 10^1 \text{ deg}$
$s103 := \sin(\phi_{\text{as}103})$	$s203 := \sin(\phi_{\text{as}203})$	$s303 := \sin(\phi_{\text{as}303})$
$s103 = 1.4382 \times 10^{-2}$	$s203 = 1.2060 \times 10^{-1}$	$s303 = 9.9979 \times 10^{-1}$
$\phi_{\text{ac}103} := \text{acos}\left(\frac{Z_1 - Z_0}{Z_3}\right)$	$\phi_{\text{ac}203} := \text{acos}\left(\frac{Z_2 - Z_0}{Z_3}\right)$	$\phi_{\text{ac}303} := \text{acos}\left(\frac{Z_3 - Z_0}{Z_3}\right)$
$\phi_{\text{ac}103} = 8.9176 \times 10^1 \text{ deg}$	$\phi_{\text{ac}203} = 8.3074 \times 10^1 \text{ deg}$	$\phi_{\text{ac}303} = 1.1826 \times 10^0 \text{ deg}$
$c103 := \cos(\phi_{\text{ac}103})$	$c203 := \cos(\phi_{\text{ac}203})$	$c303 := \cos(\phi_{\text{ac}303})$
$c103 = 1.4382 \times 10^{-2}$	$c203 = 1.2060 \times 10^{-1}$	$c303 = 9.9979 \times 10^{-1}$

FIG. 5. Phases relative to the mass gap of figure 4.

What we care about are not node phases relative to the mass gap, but rather phase differences between nodes.

$\phi_{\text{as}12} := \phi_{\text{as}103} - \phi_{\text{as}203}$	$\phi_{\text{as}13} := \phi_{\text{as}103} - \phi_{\text{as}303}$	$\phi_{\text{as}23} := \phi_{\text{as}203} - \phi_{\text{as}303}$
$\phi_{\text{as}12} = -6.1024 \times 10^0 \text{ deg}$	$\phi_{\text{as}13} = -8.7993 \times 10^1 \text{ deg}$	$\phi_{\text{as}23} = -8.1891 \times 10^1 \text{ deg}$
$s12 := \sin(\phi_{\text{as}12})$	$s13 := \sin(\phi_{\text{as}13})$	$s23 := \sin(\phi_{\text{as}23})$
$s12 = -1.0631 \times 10^{-1}$	$s13 = -9.9939 \times 10^{-1}$	$s23 = -9.9000 \times 10^{-1}$
$\phi_{\text{ac}12} := \phi_{\text{ac}103} - \phi_{\text{ac}203}$	$\phi_{\text{ac}13} := \phi_{\text{ac}103} - \phi_{\text{ac}303}$	$\phi_{\text{ac}23} := \phi_{\text{ac}203} - \phi_{\text{ac}303}$
$\phi_{\text{ac}12} = 6.1024 \times 10^0 \text{ deg}$	$\phi_{\text{ac}13} = 8.7993 \times 10^1 \text{ deg}$	$\phi_{\text{ac}23} = 8.1891 \times 10^1 \text{ deg}$
$c12 := \cos(\phi_{\text{ac}12})$	$c13 := \cos(\phi_{\text{ac}13})$	$c23 := \cos(\phi_{\text{ac}23})$
$c12 = 9.9433 \times 10^{-1}$	$c13 = 3.5015 \times 10^{-2}$	$c23 = 1.4106 \times 10^{-1}$

FIG. 6. Phases between the nodes of figure 4

Phase shifts are of same magnitude and opposite sign for sine and cosine, as required for resonance at the nodes.

Given these phase shifts, we can calculate the CKM matrix amplitudes shown in figures 2 and 10:

$-s12 \cdot c23 - c12 \cdot s23 \cdot s13 = -9.6879 \times 10^{-1}$	$c12 \cdot c23 - s12 \cdot s23 \cdot s13 = 2.4544 \times 10^{-1}$	$c23 \cdot c13 = 4.9392 \times 10^{-3}$
$s12 \cdot s23 - c12 \cdot c23 \cdot s13 = 2.4542 \times 10^{-1}$	$-c12 \cdot s23 - s12 \cdot c23 \cdot s13 = 9.6941 \times 10^{-1}$	$s23 \cdot c13 = -3.4665 \times 10^{-2}$
$s12 \cdot c13 = -3.7224 \times 10^{-3}$	$c12 \cdot c13 = 3.4817 \times 10^{-2}$	$s13 = -9.9939 \times 10^{-1}$

FIG. 7. Quark CKM matrix amplitudes in the model

Four of the phases are negative, five positive. How the signs play in the model and how they have been treated (mostly ignored) is not yet clear. Energy is square of field strength. Probabilities are squares of amplitudes.

### 3. Wolfenstein Parameters

The Wolfenstein parameters  $(\lambda, A, \rho, \eta)$  were derived as a compact and intuitive way to parametrize the CKM matrix by emphasizing hierarchical structure of quark flavor mixing, which decreases as the mass (mode energy) difference between quarks increases. The derivation relies on expanding matrix elements in powers of a small parameter  $\lambda = |V_{us}|/\sqrt{|V_{ud}|^2 + |V_{us}|^2}$ , magnitude of the mixing between the first and second generations and  $A = (1/\lambda)|V_{cb}|/|V_{us}|$  between second and third.

Hierarchical structure of the CKM matrix:

- mixing between 1st and 2nd generations is small  $\approx 0.22$
- mixing between 2nd and 3rd generations is even smaller  $\approx 0.04$
- mixing between 1st and 3rd generations is tiny  $\approx 0.004$

$$\begin{bmatrix} 1 - \frac{1}{2}\lambda^2 & \lambda & A\lambda^3(\rho - i\eta) \\ -\lambda & 1 - \frac{1}{2}\lambda^2 & A\lambda^2 \\ A\lambda^3(1 - \rho - i\eta) & -A\lambda^2 & 1 \end{bmatrix}$$

FIG. 8. Wolfenstein matrix

Expansion around small parameter  $\lambda$ :

Nicola Cabibbo first introduced the parameter  $\lambda$  to describe mixing between the first and second generations. Building on this, Wolfenstein expanded the CKM matrix in powers of  $\lambda$  and  $A\lambda^2$ , with  $\rho$  and  $\eta$  to describe relative strength of CP violation. The hierarchical structure permitted the parametrization of figure 8.

Experimental inputs:

Wolfenstein parameters are determined from experimental measurements of quark mixing processes:  $\lambda$  from kaon decays,  $A$  from B-meson decays, and  $\rho$  and  $\eta$  from rare processes involving  $|V_{ub}|$ , meson mixing  $B_d^0$  and  $B_s^0$ , and CP-violating observables.

Standard Model  $\lambda$  and  $A$  parameters are shown in blue in figure 9. They differ substantially from parameters used to calculate the impedance model Wolfenstein amplitudes. This suggests Wolfenstein analysis is not a friend of the model, that high variance  $\lambda$  and  $A$  values shown in figure 9 would not do well in generating the rest of the matrix. However, the actual fit seems remarkably good.

$$\begin{array}{lll} \lambda := \mathbf{.2250} & A := \mathbf{.0418} & \mathbf{.826} \\ \lambda := \mathbf{.2454} & A := \frac{\mathbf{.0347}}{\lambda^2} & A = \mathbf{.576} & \rho := \mathbf{.1591} & \eta := \mathbf{.3523} \\ \mathbf{V_{ud}} := 1 - \frac{\lambda^2}{2} & \mathbf{V_{us}} := \lambda & \mathbf{V_{ub}} := A \cdot \lambda^3 (\rho - i \cdot \eta) \\ \mathbf{V_{ud}} = 9.6989 \times 10^{-1} & \mathbf{V_{us}} = 2.4540 \times 10^{-1} & |\mathbf{V_{ub}}| = 3.2917 \times 10^{-3} \\ \mathbf{V_{cd}} := -\lambda & \mathbf{V_{cs}} := 1 - \frac{\lambda^2}{2} & \mathbf{V_{cb}} := A \cdot \lambda^2 \\ \mathbf{V_{cd}} = -2.4540 \times 10^{-1} & \mathbf{V_{cs}} = 9.6989 \times 10^{-1} & \mathbf{V_{cb}} = 3.4700 \times 10^{-2} \\ \mathbf{V_{td}} := A \cdot \lambda^3 [1 - (\rho - i \cdot \eta)] & \mathbf{V_{ts}} := -A \cdot \lambda^2 & \mathbf{V_{tb}} := 1 \\ |\mathbf{V_{td}}| = 7.7636 \times 10^{-3} & \mathbf{V_{ts}} = -3.4700 \times 10^{-2} & \mathbf{V_{tb}} = 1.0000 \times 10^0 \end{array}$$

FIG. 9. Wolfenstein matrix amplitudes

Figure 10 shows SM and model results of figure 2 with the Wolfenstein results appended. Bold is Standard Model, bold italic the impedance model, and plain black italic the Wolfenstein result. Impedance model result takes  $\rho$  and  $\eta$  to be zero. Wolfenstein result of figures 9 and 10 uses PDG 2024 values.

Significant differences between PDG 2024 and the model in the two inter-generational coupling constants make essentially no difference between model and remaining amplitudes of figure 10. Origin of differing amplitudes relative to the Standard Model merits further investigation. Largest relative change is in the CP violating terms, which now are in better agreement with PDG 2024. This offers the possibility of distinguishing between CP violating and QED contributions to third generation amplitudes.

<b>.9744</b>	<b>.2250</b>	<b>.0037</b>
<b>.9688</b> ud	<b>.2454</b> us	<b>.0049</b> ub
.9699	.2454	.0033
<b>.2249</b>	<b>.9735</b>	<b>.0418</b>
<b>.2454</b> cd	<b>.9694</b> cs	<b>.0347</b> cb
.2454	.9699	.0347
<b>.0086</b>	<b>.0411</b>	<b>.9991</b>
<b>.0037</b> td	<b>.0348</b> ts	<b>.9994</b> tb
.0078	.0347	1

FIG. 10. Model and Wolfenstein amplitudes

#### 4. Unitarity, Cabibbo angle, and RMS variation

Given that unitarity is a constraint in the Particle Data Group analysis, the result in figure 11 shows it has been applied faithfully to both rows (upper three) and columns (lower) in the PDG 2024 analysis. The slight variation is in the third generation. This is unlike the impedance model, which has equal and opposite variations in first and second generations. Their sum is unity at one part in one hundred thousand. Wolfenstein violates unitarity on the high side, has more coming out than going in.

PDG2024	Impedance Model	Wolfenstein
$\sqrt{.9744^2 + .2250^2 + .0037^2} = 1.0000 \times 10^0$	$\sqrt{.9688^2 + .2454^2 + .0049^2} = 9.9941 \times 10^{-1}$	$\sqrt{.9699^2 + .2454^2 + .0033^2} = 1.0005 \times 10^0$
$\sqrt{.2249^2 + .9735^2 + .0418^2} = 1.0000 \times 10^0$	$\sqrt{.2454^2 + .9694^2 + .0347^2} = 1.0006 \times 10^0$	$\sqrt{.2454^2 + .9699^2 + .0347^2} = 1.0011 \times 10^0$
$\sqrt{.0086^2 + .0411^2 + .9991^2} = 9.9998 \times 10^{-1}$	$\sqrt{.0037^2 + .0348^2 + .9994^2} = 1.0000 \times 10^0$	$\sqrt{.0078^2 + .0347^2 + 1^2} = 1.0006 \times 10^0$
$\sqrt{.9744^2 + .2249^2 + .0086^2} = 1.0001 \times 10^0$	$\sqrt{.9688^2 + .2454^2 + .0037^2} = 9.9940 \times 10^{-1}$	$\sqrt{.9699^2 + .2454^2 + .0078^2} = 1.0005 \times 10^0$
$\sqrt{.2250^2 + .9735^2 + .0411^2} = 1.0000 \times 10^0$	$\sqrt{.2454^2 + .9694^2 + .0348^2} = 1.0006 \times 10^0$	$\sqrt{.2454^2 + .9699^2 + .0347^2} = 1.0011 \times 10^0$
$\sqrt{.0037^2 + .0418^2 + .9991^2} = 9.9998 \times 10^{-1}$	$\sqrt{.0037^2 + .0348^2 + .9994^2} = 1.0000 \times 10^0$	$\sqrt{.0078^2 + .0347^2 + 1^2} = 1.0006 \times 10^0$

FIG. 11. Unitarity for the results of figure 10

RMS variance with PDG 2024 is slightly more than one percent for both; for the model 0.0105 and for Wolfenstein parameterization 0.0103, a small but possibly significant improvement.

$$\frac{\sqrt{.0056^2 + .0204^2 + .0012^2 + .0205^2 + .0041^2 + .0071^2 + .0049^2 + .0063^2 + .0003^2}}{\sqrt{9}} = 1.0542 \times 10^{-2}$$

$$\frac{\sqrt{.0045^2 + .0204^2 + .0004^2 + .0205^2 + .0036^2 + .0071^2 + .0008^2 + .0064^2 + .0009^2}}{\sqrt{9}} = 1.0342 \times 10^{-2}$$

FIG. 12. RMS variance for impedance model and Wolfenstein analysis

$$\tan\phi_c := \frac{.2249}{.9735} \quad \phi_c := \text{atan}(\tan\phi_c) \quad \phi_c = 1.3008 \times 10^1 \text{ deg}$$

$$\tan\phi_c := \frac{.2454}{.9694} \quad \phi_c := \text{atan}(\tan\phi_c) \quad \phi_c = 1.4206 \times 10^1 \text{ deg}$$

FIG. 13. Cabibbo angle

In both model and Wolfenstein analysis, the largest contributors to variance are  $V_{us}$  of Cabibbo mixing between first and second generations, and  $V_{cb}$  between second and third. The model gives a Cabibbo angle that differs by about one degree from the data.

## 5. CP violation: spin, dimensionality, and topology

Components of the largest normed *division* algebra (topology requires inversion), the Pauli algebra of 3D space, are those of the impedance model vacuum wavefunction - one scalar, three vector lines (orientational degrees of freedom), three bivector areas, and one trivector volume (1,3,3,1) [16]. This is Geometric Algebra, the Clifford algebra of geometric objects [17–20]. Unlike matrix representations of Pauli and Dirac, in geometric representation the wavefunction is easily visualized.

Wavefunction interactions are modeled by dimension-changing Clifford products of figure 14, sum of dot and wedge. Product of two vectors is scalar plus bivector,  $WZ = Higgs + top$ . Like the 60s S-matrix bootstrap, there is no Lagrangian. Equations of motion calculate the impedance networks [13, 21].

Physical manifestation of the vacuum wavefunction arises from introducing the coupling constant  $\alpha = e^2/4\pi\epsilon_0\hbar c$ . Various combinations of the four fundamental constants that define  $\alpha$  permit assigning geometrically and topologically appropriate electric and magnetic flux quanta to the eight wavefunction components [15, 22].

The point is that these are the objects whose interactions we seek to visualize to understand CPT symmetries. However, in the presence of topology and spin inherent in dimension-changing Clifford product interactions, there remain things not properly understood. While the ability to visualize wavefunction interactions in real 3D space is a huge advantage over the more abstract Standard Model perspective, how spin, dimensionality, and topology play in the model remains unclear [23]. Details of CP violation in the impedance model are ignored in the present work, hopefully to be addressed in the near future, along with the neutrino mixing matrix.

## 6. Topological calculation of $\pi^0$ , $\eta$ , and $\eta'$ branching ratios

The  $\pi^0$  branching ratio calculation [9] was motivated by Michael Creutz [24–26], who upon first seeing  $\pi^0$  in the ‘One Slide’ of figure 4, said “The chiral anomaly” [25].

The anomaly arises from the need to **regularize** the quantum field theory, which breaks classical symmetries.

### The $\pi^0$ Branching Ratios

The relatively simple  $\pi^0$  branching tree is shown in figure 3. As the image suggests, the impedance calculation is done taking the paths in parallel.

As shown in figure 2, the  $\pi^0$  coherence length coincides with the (inverse) Rydberg, where there is an impedance match via the dipole mode. Ignoring the phases, the impedance of the two photon decay can be written as

$$Z_{\gamma\gamma} = \frac{1}{\frac{1}{Z_0} + \frac{1}{Z_0}} = \frac{Z_0}{2} = 188.37 \Omega \quad (1)$$

and that of the  $e^+e^-\gamma$  mode as

$$Z_{ee\gamma} = \frac{1}{\frac{1}{R_H} + \frac{1}{R_H} + \frac{4\alpha^2}{Z_0}} = \frac{Z_0}{4\alpha^2 + 4\alpha} = 12813 \Omega \quad (2)$$

where  $R_H = \frac{Z_0}{2\alpha}$  is the quantum Hall resistance, so that

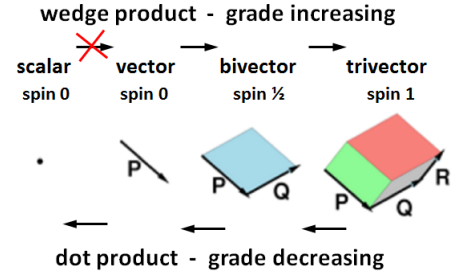


FIG. 14. Pauli algebra of 3D space

$$Z_{\pi^0} = \frac{1}{\frac{1}{Z_{\gamma\gamma}} + \frac{1}{Z_{ee\gamma}}} = \frac{Z_0}{4\alpha^2 + 4\alpha + 2} = 185.64 \Omega \quad (3)$$

and the branching ratios are

$$\Gamma_{\gamma\gamma} = \frac{Z_{\pi^0}}{Z_{\gamma\gamma}} = \frac{1}{2\alpha^2 + 2\alpha + 1} = 0.9855 (0.988) \quad (4)$$

$$\Gamma_{ee\gamma} = \frac{Z_{\pi^0}}{Z_{ee\gamma}} = \frac{2\alpha^2 + 2\alpha}{2\alpha^2 + 2\alpha + 1} = 0.0145 (0.012) \quad (5)$$

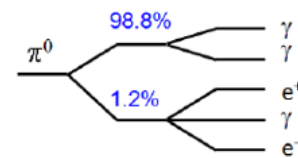


FIG. 3. The  $\pi^0$  branching tree

FIG. 15. Quantum Impedance Networks are Feynman’s **Regulators**

Bjorken discovered the electromagnetic circuit analog of Feynman's *regulators*, anticipated it offering a powerful intuitive perspective. [27–29]. He was thwarted by topological inversion in our systems of units, understood more [kg/s] to mean more flow, *conductance*. However in SI units [kg/s] is mechanical *impedance*. More [kg/s] means more impedance, less flow. The resulting confusion confounded intuition, continues to do so to this day.

The model contains topological inversion (the division algebra requirement satisfied by Clifford) that obstructed Bjorken and the many of us who followed. Inversion arises from magnetic charge, topological dual of scalar electric charge [30, 31]), trivector pseudoscalar in the (1,3,3,1) mass gap wavefunction. Energy of Dirac's magnetic charge quantum when confined to the electron Compton wavelength is .511 MeV. Energy of electric charge is .511 MeV at the classical radius of figure 4, 137 times smaller.

With electric charge, fundamental lengths at top right of figure 4 correspond to specific mechanisms of photon emission or absorption, matched in both quantized impedance and energy. Inversion results in mismatches in both. Magnetic charge is 'dark', cannot couple to the photon, not despite its great strength, but rather because of it. The  $\alpha$ -spaced lengths of figures 3 and 4 correspond to physical mechanisms. Bohr radius cannot be inside Compton wavelength in the basic photon-charge coupling of QED, Rydberg cannot be inside Bohr,... Specific physical mechanisms of photon emission and absorption no longer work. Magnetic charge is topological, dark.

Impedance networks are finite without renormalization. Inductance of the singularity is infinite, capacitance nil. In the boundary at infinity, capacitance infinite and inductance nil. We are decoupled by the infinite mismatch. All energy/information is reflected back. It is this naturally [22] finite property of the model that permits the simple branching ratio calculation of figure 15, made possible the  $\eta$  and  $\eta'$  result, and *removed the anomaly*.

Impedance networks are finite without renormalization. Inductance of the singularity is infinite, capacitance nil. In the boundary at infinity, capacitance infinite and inductance nil. We are decoupled by the infinite mismatch. All energy/information is reflected back. It is this naturally [22] finite property of the model that permits the simple branching ratio calculation of figure 15, made possible the  $\eta$  and  $\eta'$  result, and *removed the anomaly*.

Coming back to the branching ratio calculation of  $\eta$ :

### The $\eta$ Branching Ratios

The more complex  $\eta$  branching tree is shown in figure 4. Here we follow the same method as in the previous example, working from top to bottom and right to left in the figure as we calculate. Again ignoring the phases, as well as factors of two that will be addressed in the discussion that follows, the impedance of the two photon decay can be written as

$$Z_{\gamma\gamma} = \frac{1}{\frac{2}{Z_0} + \frac{2}{Z_0}} = \frac{Z_0}{4} \quad (6)$$

The  $\pi^0$  impedance calculated in the previous section is

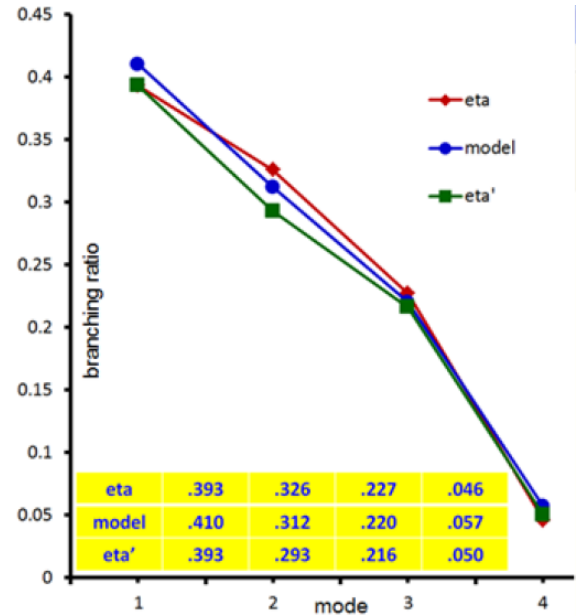


FIG. 16. Data and Model

used to find that of the three  $\pi^0$  decay

$$Z_{3\pi^0} = \frac{2}{\frac{1}{Z_{\pi^0}} + \frac{1}{Z_{\pi^0}} + \frac{1}{Z_{\pi^0}}} = \frac{2Z_0}{3(4\alpha^2 + 4\alpha + 2)} \quad (7)$$

We assume the neutrino has rest mass, and therefore a scale invariant centrifugal impedance

$$Z_\nu = R_H = \frac{Z_0}{2\alpha} \quad (8)$$

so that the muon impedance is

$$Z_\mu = \frac{1}{\frac{1}{Z_e} + \frac{1}{Z_\nu} + \frac{1}{Z_\nu}} = \frac{R_H}{3} = \frac{Z_0}{6\alpha} \quad (9)$$

The impedances of the charged pions are then

$$Z_{\pi^+} = Z_{\pi^-} = \frac{1}{\frac{1}{Z_\nu} + \frac{1}{Z_\mu}} = \frac{Z_0}{8\alpha} \quad (10)$$

FIG. 17. Equation 9 calculates muon impedance. Difference between  $\eta$  and  $\eta'$  in figure 16 is  $3\pi^0$  decay of equations 7 and 15.

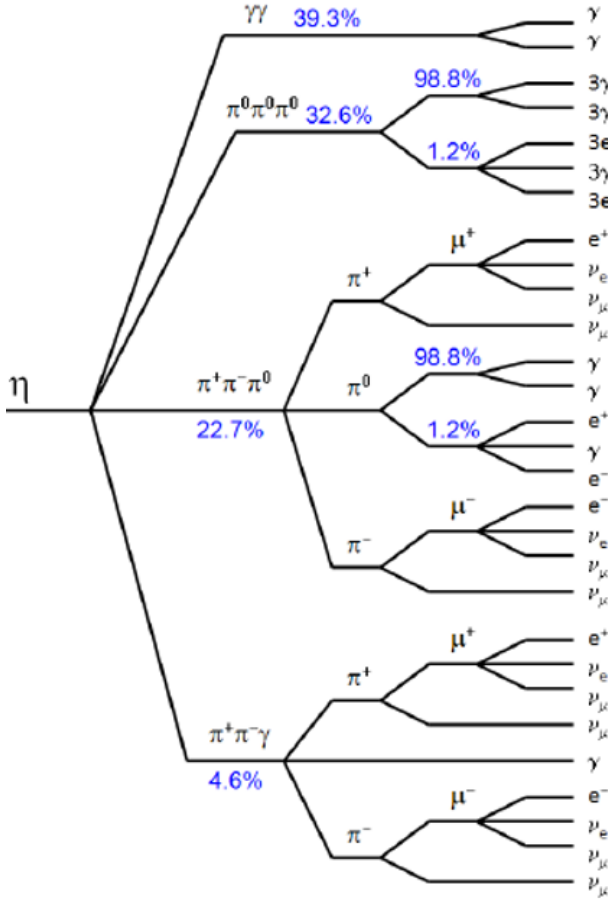


FIG. 4. The  $\eta$  branching tree

FIG. 18. The  $\eta$  branching ratio calculation in powers of the electromagnetic coupling constant  $\alpha$ .

The  $\eta$  calculation does a remarkably good job of matching both  $\eta$  and  $\eta'$  branching ratios of figure 16, has an RMS variance from experiment of about one part in one hundred for both. This despite the network structure of figure 4 being significantly different between mass gap Compton wavelength of  $\eta'$  and Bohr radius of  $\eta$ . Why this is so is not yet clear in the impedance model. One possibly useful consideration takes into account the flow of energy from left to right during figure 4 decays. Hopefully the Standard Model can offer some insight.

## 7. Summary

Each of the previous six sections is briefly summarized:

**Introduction** - Presented a brief outline of the quark mixing matrix and a first look at the impedance model result.

**CKM matrix impedance calculation** - Introduced the four quantum impedances generated by  $Z_0$ , the 377 ohm impedance the photon excites in free space, raised to powers of twice the coupling constant  $\alpha$ , their place in the ‘One Slide’ quantum impedance network, and details of a calculation that ignored CP violation.

and the impedance of the  $\pi^+\pi^-\pi^0$  decay is

$$Z_{\pi\pi\pi^0} = \frac{1}{\frac{1}{Z_{\pi^+}} + \frac{1}{Z_{\pi^-}} + \frac{1}{Z_{\pi^0}}} = \frac{Z_0}{4\alpha^2 + 20\alpha + 2} \quad (11)$$

Finally, the impedance of the  $\pi^+\pi^-\gamma$  decay is

$$Z_{\pi\pi\gamma} = \frac{2}{\frac{1}{Z_{\pi^+}} + \frac{1}{Z_{\pi^-}} + \frac{1}{Z_0}} = \frac{2Z_0}{16\alpha + 1} \quad (12)$$

so that the impedance of the  $\eta$  is

$$Z_\eta = \frac{1}{\frac{1}{Z_{\gamma\gamma}} + \frac{1}{Z_{3\pi^0}} + \frac{1}{Z_{\pi^+\pi^-\pi^0}} + \frac{1}{Z_{\pi^+\pi^-\gamma}}} \quad (13)$$

$$= \frac{2Z_0}{20\alpha^2 + 68\alpha + 19}$$

and the branching ratios are

$$\Gamma_{\gamma\gamma} = \frac{Z_\eta}{Z_{\gamma\gamma}} = \frac{8}{20\alpha^2 + 68\alpha + 19} \quad (14)$$

$$= 0.410 (0.393)$$

$$\Gamma_{3\pi^0} = \frac{Z_\eta}{Z_{3\pi^0}} = \frac{3(4\alpha^2 + 4\alpha + 2)}{20\alpha^2 + 68\alpha + 19} \quad (15)$$

$$= 0.312 (0.326)$$

$$\Gamma_{\pi\pi\pi^0} = \frac{Z_\eta}{Z_{\pi\pi\pi^0}} = \frac{2(4\alpha^2 + 20\alpha + 2)}{20\alpha^2 + 68\alpha + 19} \quad (16)$$

$$= 0.220 (0.227)$$

$$\Gamma_{\pi\pi\gamma} = \frac{Z_\eta}{Z_{\pi\pi\gamma}} = \frac{16\alpha + 1}{20\alpha^2 + 68\alpha + 19} \quad (17)$$

$$= 0.057 (0.046)$$

Again, codata 2010 values are shown in parentheses.

**Wolfenstein parameters** - Outlined the hierarchical structure of quark flavor mixing as a tool for gaining intuitive understanding of the CKM matrix, presented Wolfenstein analysis of the impedance model, and used PGD 2024 parameter values for  $\rho$  and  $\eta$  to offer the possibility of distinguishing between QED and CP violation contributions to third generation amplitudes.

**Unitarity, Cabibbo angle, and RMS variation** - Sum of the model unitarities is unity at one part in one hundred thousand. Cabibbo angle is about one degree larger than Standard Model. RMS variance of model amplitudes relative to the Standard Model is about one part in one hundred.

**CP violation: spin, dimensionality, and topology** - Introduced the vacuum wavefunction (same at all scales) and physical manifestation via various combination of the four fundamental constants that define the electromagnetic coupling constant  $\alpha = e^2/4\pi\epsilon_0\hbar c$ . Different physics at different scales arises from scale at which invariant flux quanta are confined, at a given Compton wavelength node, by coherent impedance mismatch reflections as fields seek to propagate away. Outlined how spin, dimensionality, and topology play with CPT symmetries in the model.

**Topological QED calculation of  $\pi^0, \eta$ , and  $\eta'$  branching ratios** - RMS variation of the model results relative to the Standard Model is about two parts per thousand for  $\pi^0$ , and one part in one hundred for  $\eta$  and  $\eta'$

## 8. Conclusion

“The hard part will be getting physicists to think in terms of impedances”

Richard Talman, walking to lunch at Brookhaven (2012)

While the quark mixing matrix calculation appears compelling, when buttressed by the  $\pi^0, \eta$ , and  $\eta'$  branching ratios it gains ever more serious credibility. Both are founded and fortified by the figure 4 One Slide calculation [11–13, 21, 32–34], by correlation between mass gap network nodes and unstable particle causal coherence lengths that explain lifetimes and confinement. These three calculations, like almost all impedance model results [35, 36], are of a phenomenology alien to the theorist, cognitively dissonant, too different to resonate. Like the 1960s S-matrix bootstrap (progenitor of string theory), the model has no Lagrangian. Equations of motion directly calculate the impedance networks. These govern amplitude and phase of energy flow, of information transmission.

The hope is that, in this one short note, these three calculations inspire a few curious minds to foresake some portion of canonical comfort in exchange for an outlier [37], to dive down the rabbit hole and find safe space, and there to organize systematic examination and extrapolation of not only the model, but also the lifetime enhancement conjecture. Of immediate interest is gauge fixing of the neutrino mixing matrix, where an amplitudes calculation of simplicity and precision seen in the quark mixing result could give guidance to theorists and experimentalists, promoting “neutrino science, dark matter experiments, muons and the muon collider, and new physics ideas’ [38].

## 8. Acknowledgments

The author thanks family and friends for unfailing support and encouragement, and GPT4o for guidance in writing introductions to the CKM matrix and Wolfenstein parametrization.

## Supplementary Material

Bottom line of this work with CKM and PMNS is to understand muon and neutrino wavefunctions of figures 20 and 21, and how (if possible) to introduce appropriate impedances to muon collider lattices for the purpose of prolonging muon lifetime, particularly at low energy [6, 7].

The three components that comprise the 1D vector, 2D bivector, and 3D trivector (1,2,3) neutrino wavefunction and the resulting nine S-matrix modes generated by geometric Clifford products are indicated by ellipses in figure 19. Modes indicated by symbols (triangle, square,...) are plotted in the One Slide of figure 4, including the off-diagonal scalar Lorentz neutrino eigenmode (red triangles in both figures), a scale-dependent geometric impedance it shares with on-diagonal (red squares) magnetic Coulomb mode in the quark mixing matrix.

	electric charge $e$ scalar	elec dipole moment 1 $d_{E1}$ vector	elec dipole moment 2 $d_{E2}$ vector	mag flux quantum $\Phi_B$ vector	elec flux quantum 1 $\Phi_{E1}$ bivector	elec flux quantum 2 $\Phi_{E2}$ bivector	magnetic moment $\mu_B$ bivector	magnetic charge $g$ trivector
$e$	$ee$ scalar	$ed_{E1}$	$ed_{E2}$ vector	$e\Phi_B$	$e\Phi_{E1}$	$e\Phi_{E2}$ bivector	$e\mu_B$	$eg$ trivector
$d_{E1}$	$d_{E1}e$	$d_{E1}d_{E1}$	$d_{E1}d_{E2}$	$d_{E1}\Phi_B$	$d_{E1}\Phi_{E1}$	$d_{E1}\Phi_{E2}$	$d_{E1}\mu_B$	$d_{E1}g$
$d_{E2}$	$d_{E2}e$	$d_{E2}d_{E1}$	$d_{E2}d_{E2}$	$d_{E2}\Phi_B$	$d_{E2}\Phi_{E1}$	$d_{E2}\Phi_{E2}$	$d_{E2}\mu_B$	$d_{E2}g$
$\Phi_B$	$\Phi_B e$ vector	$\Phi_B d_{E1}$	$\Phi_B d_{E2}$ scalar + bivector	$\Phi_B \Phi_B$	$\Phi_B \Phi_{E1}$ Y	$\Phi_B \Phi_{E2}$ vector + trivector	$\Phi_B \mu_B$	$\Phi_B g$ bv + qv
$\Phi_{E1}$	$\Phi_{E1} e$ ▲	$\Phi_{E1} d_{E1}$	$\Phi_{E1} d_{E2}$	$\Phi_{E1} \Phi_B$ Y	$\Phi_{E1} \Phi_{E1}$	$\Phi_{E1} \Phi_{E2}$	$\Phi_{E1} \mu_B$	$\Phi_{E1} g$ ●
$\Phi_{E2}$	$\Phi_{E2} e$ ▲	$\Phi_{E2} d_{E1}$	$\Phi_{E2} d_{E2}$	$\Phi_{E2} \Phi_B$	$\Phi_{E2} \Phi_{E1}$	$\Phi_{E2} \Phi_{E2}$	$\Phi_{E2} \mu_B$	$\Phi_{E2} g$ ●
$\mu_B$	$\mu_B e$ bivector	$\mu_B d_{E1}$	$\mu_B d_{E2}$ vector + trivector	$\mu_B \Phi_B$	$\mu_B \Phi_{E1}$	$\mu_B \Phi_{E2}$ scalar + quadvector	$\mu_B \mu_B$	$\mu_B g$ vector + pv
$g$	$ge$ trivector	$gd_{E1}$	$gd_{E2}$ bivector + quadvector	$g\Phi_B$	$g\Phi_{E1}$	$g\Phi_{E2}$ vector + pentavector	$g\mu_B$	$gg$ scalar + sv

FIG. 19. S-matrix at the QED mass gap, eigenmodes in blue, transition in yellow, fermions and bosons, flavor and color.

In the model the neutrino is a photon comprised of 1D magnetic and 2D electric flux quanta, which sit on the skew diagonal with the color SU(3) gluons of figure 19, adjacent the main diagonal. They are coupled by Maxwell's equations, mixing with and topologically protected by 3D magnetic charge (1,2,3). Additionally, all nine modes in the three-by-three neutrino S-matrix of figure 20 are degenerate, respecting the definition of topological protection.

In SI units the spin 0 1D vector magnetic flux quantum of the photon and spin 1 3D trivector Dirac magnetic charge are the same,  $\Phi_B = h/2e = g$ . This despite the fact that they are geometrically and topologically distinct. They excite the vacuum differently, experience differential phase shifts of massless neutrino oscillation.

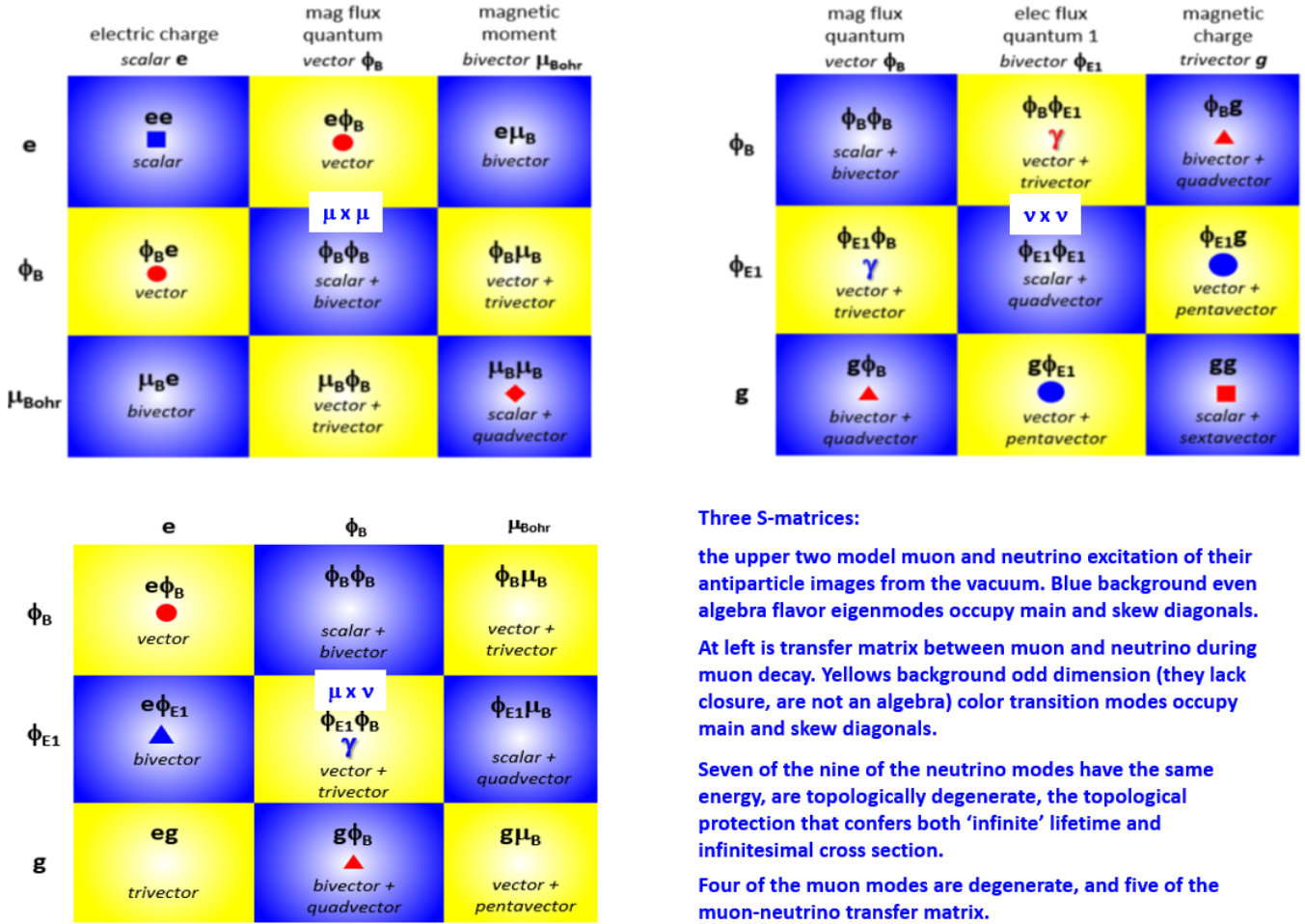


FIG. 20. Muon and neutrino wavefunctions and S-matrices, and their transfer matrix during muon decay.

The 1D vector  $W$  of figure 21 doesn't appear in figure 20 S-matrices. It barely exists, decays in  $\approx 10^{-25}$  seconds, at light speed propagates a mere  $\approx 10^{-4}$  electron Compton wavelength, cannot be causal other than to facilitate the change in real space dimensionality of the decay. What does appear in  $\mu$ ,  $\nu_\mu$ , and  $\nu_e$  wavefunctions is the 1D vector magnetic flux quantum  $\Phi_B$ . Vector magnetic flux quantum and trivector magnetic charge are defined identically,  $\Phi_B = h/2e = g$ , despite the fact that they are geometrically and topologically distinct. Absence of the muon vector  $\Phi_B$  magnetic dipole flux quantum dipole component, with its poles at infinity (and distinct from the axial bivector Bohr magneton), in the decay products can be thought of as the topological balance to loss of dimensionality [23]. One might imagine  $\phi_B$  in superposition with magnetic charge  $g$ , and coupled with electric charge of the dyon [39] during decay of the  $W$ .

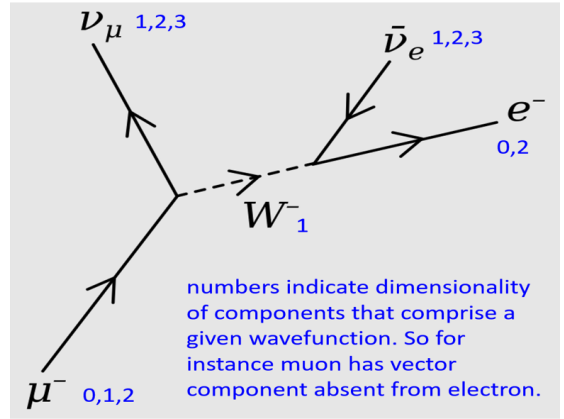


FIG. 21. Muon decay

- 
- [1] P. Ramond, “The case for a Family Symmetry”, Workshop: Future Prospects for Fundamental Particle Physics and Cosmology, Simons Center, Stony Brook (2015) [https://scgp.stonybrook.edu/video\\_portal/video.php?id=535](https://scgp.stonybrook.edu/video_portal/video.php?id=535)
- [2] P. Ramond, private communication (2020)
- [3] <https://pdg.lbl.gov/2024/reviews/rpp2024-rev-neutrino-mixing.pdf>
- [4] <https://pdg.lbl.gov/2024/reviews/rpp2024-rev-ckm-matrix.pdf>
- [5] C. Rubbia, “A Call for Courage as Physicists Confront Collider Dilemma”, Quanta magazine (2019). <https://www.quantamagazine.org/carlo-rubbia-calls-for-courage-as-physicists-confront-collider-dilemma-20190807/>
- [6] P. Cameron, “Sustaining Wavefunction Coherence via Topological Impedance Matching: Stable Polarized Muon Beams at 255 x 255 GeV/c?” (2020) <http://dx.doi.org/10.13140/RG.2.2.35153.61282>
- [7] P. Cameron, “Bootstrapping the Muon Collider: Massless Neutrinos in the g-2 Delivery Ring”, Snowmass White Paper (2022) <http://dx.doi.org/10.13140/RG.2.2.21469.69603/1>
- [8] K.M. Black et.al., “Muon Collider Forum Report”, Snowmass (2022) <https://doi.org/10.48550/arXiv.2209.01318>
- [9] P. Cameron, “Impedance Approach to the Chiral Anomaly” (2014) <http://dx.doi.org/10.13140/RG.2.2.22417.10081>
- [10] S. Coon and B. Holstein, “Anomalies in Quantum Mechanics: the  $1/r^2$  Potential”, Am.J.Phys. **70**, 513 (2002) <http://arxiv.org/abs/quant-ph/0202091v1>
- [11] M. MacGregor, “The Fine-Structure Constant as a Universal Scaling Factor”, Lett. Nuovo Cimento **1**, 759-764 (1971)
- [12] M. MacGregor, *The Power of Alpha*, World Scientific (2007)
- [13] P. Cameron, “Electron Impedances”, Apeiron **18** 2 p.222-253 (2011) <http://redshift.vif.com/JournalFiles/V18N02PDF/V18N2CAM.pdf>
- [14] P. Cameron, “Generalized Quantum Impedances: A Background Independent Model for the Unstable Particle Spectrum” (2012) <http://dx.doi.org/10.13140/RG.2.2.25702.84800>
- [15] See the appended supplementary material for wavefunction components and S-matrices of wavefunction interactions.
- [16] D. Hestenes, *Space-Time Algebra*, Gordon and Breach, New York (1966)
- [17] W. Clifford, “Applications of Grassmann’s extensive algebra”, Am. J. Math., **1** 350 (1878)
- [18] D. Hestenes, “Oersted Medal Lecture 2002: Reforming the mathematical language of physics”, Am. J. Phys. **71**, 104 (2003) <http://geocalc.clas.asu.edu/pdf/OerstedMedalLecture.pdf>
- [19] D. Hestenes, “The Genesis of Geometric Algebra: A Personal Retrospective”, Adv. Appl. Clifford Algebras **27** (2017) <https://link.springer.com/article/10.1007/s00006-016-0664-z>
- [20] C. Doran and A. Lasenby, *Geometric Algebra for Physicists*, Cambridge University Press (2003)
- [21] P. Cameron, “How to: Calculating Quantum Impedance Networks” <http://dx.doi.org/10.13140/RG.2.2.32166.65601>
- [22] P. Cameron and M. Suisse, “Naturalness begets Naturalness: An Emergent Definition” (2019) <http://dx.doi.org/10.13140/RG.2.2.13602.20165>
- [23] P. Cameron, “Spin, Dimensionality, and Topology in the Fano Plane”, XXV High Energy Phys. Symp., India (2023) <http://dx.doi.org/10.13140/RG.2.2.18079.64164>  
<https://www.youtube.com/watch?v=LAjQSRoFwgg&t=12s>

- [24] M. Creutz, “*Quarks, Gluons and Lattices*”, Cambridge University Press (1983)
- [25] M. Creutz, private communication (2012)
- [26] M. Creutz, “The Standard Model and the Lattice” (2023) <https://arxiv.org/abs/2310.00061>
- [27] J. Bjorken, “Experimental tests of quantum electrodynamics and spectral representations of Green’s functions in perturbation theory”, Thesis, Dept. of Physics, Stanford (1959) <http://searchworks.stanford.edu/view/2001021>
- [28] J. Bjorken, private communication (2013)
- [29] J. Bjorken, and S. Drell, *Relativistic Quantum Fields*, McGraw-Hill, section 18.4 (1965)
- [30] N. Seiberg and E. Witten, “Monopoles, duality and chiral symmetry breaking in N=2 supersymmetric QCD”, Nucl. Phys. B. 431 (3): 484–550 (1994). <https://arxiv.org/abs/hep-th/9408099>
- [31] E. Witten, “Duality, Spacetime, and Quantum Mechanics”, Physics Today (May 1997)
- [32] P. Cameron, “The Two Body Problem and Mach’s Principle”, submitted to AJP, in revision. (1975)  
Published as an appendix to the Electron Impedances paper [13].
- [33] P. Cameron, “Genesis of a Quantum Impedance Model”, March 2023 APS annual meeting.  
<https://www.youtube.com/watch?v=cvK6TxKRmI8>
- [34] P. Cameron, “Not Your Father’s Physics”, essay written for the 2024 APS History of Physics Essay Competition.  
<http://dx.doi.org/10.13140/RG.2.2.15558.08004>
- [35] [https://www.researchgate.net/profile/Peter-Cameron-3?ev=hdr\\_xprf](https://www.researchgate.net/profile/Peter-Cameron-3?ev=hdr_xprf)
- [36] [https://vixra.org/author/peter\\_cameron](https://vixra.org/author/peter_cameron)
- [37] M. Gladwell, *Outliers - the Story of Success*, Back Bay Books, NY (2008).
- [38] P. Cameron, “Quantum Impedance Networks and the Fermilab Accelerator Complex Evolution”,  
Fermilab ACE Science Workshop (2023) <http://dx.doi.org/10.13140/RG.2.2.35402.17608>
- [39] <https://en.wikipedia.org/wiki/Dyon>